Journal of Rock Mechanics and Geotechnical Engineering 10 (2018) 879–892

Contents lists available at ScienceDirect

Journal of Rock Mechanics and Geotechnical Engineering

journal homepage: www.rockgeotech.org

Full Length Article

A discrete model for prediction of radon flux from fractured rocks

K.M. Ajayi [a,*], K. Shahbazi [a], P. Tukkaraja [b], K. Katzenstein [c]

[a] Department of Mechanical Engineering, South Dakota School of Mines and Technology, Rapid City, SD, 57701, USA
[b] Department of Mining Engineering and Management, South Dakota School of Mines and Technology, Rapid City, SD, 57701, USA
[c] Department of Geology and Geological Engineering, South Dakota School of Mines and Technology, Rapid City, SD, 57701, USA

ARTICLE INFO

Article history:
Received 3 January 2018
Received in revised form
18 February 2018
Accepted 22 February 2018
Available online 27 July 2018

Keywords:
Radon mass flux
Radon dimensionless flux
Stochastic model
Discrete fracture network (DFN)
Caving mining method
Fractured rocks

ABSTRACT

Prediction of radon flux from the fractured zone of a propagating cave mine is basically associated with uncertainty and complexity. For instance, there is restricted access to these zones for field measurements, and it is quite difficult to replicate the complex nature of both natural and induced fractures in these zones in laboratory studies. Hence, a technique for predicting radon flux from a fractured rock using a discrete fracture network (DFN) model is developed to address these difficulties. This model quantifies the contribution of fractures to the total radon flux, and estimates the fracture density from a measured radon flux considering the effects of advection, diffusion, as well as radon generation and decay. Radon generation and decay are classified as reaction processes. Therefore, the equation solved is termed as the advection-diffusion-reaction equation (ADRE). Peclet number (*Pe*), a conventional dimensionless parameter that indicates the ratio of mass transport by advection to diffusion, is used to classify the transport regimes. The results show that the proposed model effectively predicts radon flux from a fractured rock. An increase in fracture density for a rock sample with uniformly distributed radon generation rate can elevate radon flux significantly compared with another rock sample with an equivalent increase in radon generation rate. In addition to *Pe*, two other independent dimensionless parameters (derived for radon transport through fractures) significantly affect radon dimensionless flux. Findings provide insight into radon transport through fractured rocks and can be used to improve radon control measures for proactive mitigation.

© 2018 Institute of Rock and Soil Mechanics, Chinese Academy of Sciences. Production and hosting by Elsevier B.V. This is an open access article under the CC BY-NC-ND license (http://creativecommons.org/licenses/by-nc-nd/4.0/).

1. Introduction

Radon gas is a major source of ionizing radiation (Nadakavukaren, 2011), emitting harmful radioactivity during its decay (McPherson, 1993). The Health Protection Agency (HPA) estimates that about 1100 radon-induced lung cancer deaths occur every year in UK (HPA, 2009), and the Environmental Protection Agency (EPA) estimates that about 21,000 radon-related lung cancer deaths occur each year in the US (US EPA, 2017). These problems are more severe around uranium-rich rocks (El-Fawal, 2011), because radon is a disintegration product from uranium (Barakos et al., 2014), known to be abundant in rare-earth minerals (Abumurad and Al-Tamimi, 2001). In addition, certain mining methods such as caving mining, which involves inducing fracturing of rock (McNearny and Abel, 1993; Li et al., 2014), increases rock's surface area and creates pathways for radon gas to migrate within the rock mass. This makes prediction of radon flux more complex in the caving mining of uranium-rich rocks.

Radon (discharged by radium-bearing molecules) migrates within the rock mass (Ferry et al., 2002) by diffusion and/or advection through pores, macro-pores, and fractures (Nazaroff and Nero, 1988; Ferry et al., 2002), and eventually emanates into the atmosphere. In a steady flow situation in a rock mass, fractures transport 99.99% of the total vertical mass flow through the composite medium (Nilson et al., 1991). Therefore, fractures contribute significantly to radon transport (Schery et al., 1982; Holford et al., 1993; Rowberry et al., 2016) and to proactively mitigating human exposure to radon. In this sense, knowledge of radon flux is required. At present, there are a few traditional approaches for predicting radon flux, but they are not relevant in all cases. One approach is the direct measurement of radon flux in houses and mines (Lario et al., 2005; Kitto, 2014; Ongori et al., 2015). For this approach, Lario et al. (2005) concluded that only uninterrupted

* Corresponding author.
E-mail address: kayode.ajayi@mines.sdsmt.edu (K.M. Ajayi).
Peer review under responsibility of Institute of Rock and Soil Mechanics, Chinese Academy of Sciences.

https://doi.org/10.1016/j.jrmge.2018.02.009
1674-7755 © 2018 Institute of Rock and Soil Mechanics, Chinese Academy of Sciences. Production and hosting by Elsevier B.V. This is an open access article under the CC BY-NC-ND license (http://creativecommons.org/licenses/by-nc-nd/4.0/).

short-term monitoring can represent radon concentration over an extended period. However, this approach is not relevant for rocks with access constraints, such as cave mines. Another approach used is laboratory investigation. Sahu et al. (2013) conducted a laboratory test of radon emanation rate from a low-grade uranium ore sample and found that in situ radon emanation rate is about 3 times higher than that measured in the laboratory. This disparity is attributed to the massive size and degree of fracturing in in situ orebodies (Bochiolo et al., 2012; Sahu et al., 2013), which is difficult to be replicated in laboratory studies. These challenges limit the application of these techniques. Hence, a non-traditional strategy is required to predict radon flux for large-scale underground excavations.

We developed an approach for predicting radon flux from fractured rocks, a discrete fracture network (DFN) model that can predict radon transport through fractures considering diffusion, advection, and radon generation with radon decay. We assumed that radon flux at the rock's surface is due to the transport by advection and diffusion (Catalano et al., 2015) through the fractures. Multiple studies predict that advection dominates radon transport (Nilson et al., 1991; Rowberry et al., 2016) (diffusion can be ignored); however, within the range of radon diffusion length (2.18 m) (Thompkins, 1982) and for rocks with low permeability, both are important (Bear et al., 1993; Mosley et al., 1996). The influence of diffusion transport is limited by its short half-life (3.83 d), but advection transport through structural discontinuities can cover about 100 m length more than diffusion (Appleton, 2013).

We solved the advection-diffusion-reaction equation (ADRE), where radon generation and decay are classified as reaction processes. This requires the knowledge of advection velocity (u) and we used three different methods to compute u. The technique developed in this study applies to fractured rock and specifically to instances such as a propagating cave mine, where the yield, seismogenic, and elastic zones (Board and Pierce, 2009; Sainsbury, 2010) (characterized by both natural and induced fractures) are inaccessible for field measurements.

2. Research approach

2.1. Radon flux

2.1.1. Radon flux from a rock mass

Advection and diffusion are the major transport mechanisms for a rock mass (Cigna, 2005; Prasad et al., 2012; Ye et al., 2014; Catalano et al., 2015). Therefore, radon flux (J) is obtained by summing the flux due to advection and diffusion. The flux due to diffusion (J_{diff}) is derived using Fick's first law of diffusion:

$$J_{\text{diff}} = -D\frac{\partial c}{\partial z} \tag{1}$$

and the flux due to advection (J_{adv}) is obtained (Garges and Baehr, 1998) using

$$J_{\text{adv}} = uc \tag{2}$$

where D is the radon's coefficient of molecular diffusion (m^2/s), c is the radon concentration (Bq/m^3), z is the fracture axis, and u is the advection velocity (m/s).

2.1.2. Radon concentration for a single fracture

Radon concentration (c), required for Eqs. (1) and (2), is obtained from radon transport equation (Bates and Edwards, 1980; Bear et al., 1993; Mosley et al., 1996):

$$\frac{\partial c}{\partial t} = \nabla\cdot(D\nabla c) - \nabla\cdot(Vc) - \lambda c + q \tag{3}$$

where λ is the decay constant (s^{-1}), t is the time (s), V is the fluid velocity (m/s), and q is the radon generation rate ($Bq/(m^3\ s)$). For fractures in the rock mass, q is the radon flux from the fracture walls per unit aperture and is assumed to be uniform. Assuming a steady, incompressible and one-dimensional transport of radon along the fracture axis (z), Eq. (3) is reduced (Iakovleva and Ryzhakova, 2003; Xie et al., 2012; Zhang et al., 2014) to

$$D\frac{\partial^2 c}{\partial z^2} - u\frac{\partial c}{\partial z} - \lambda c + q = 0 \tag{4}$$

Eq. (4) is non-dimensionalized by using $c^* = c/c_\infty$ and $z^* = z/L$, where L is the characteristic length of the DFN size, and c_∞ is the reference concentration. Then we have

$$\frac{d^2c^*}{dz^{*2}} - \frac{uL}{D}\frac{dc^*}{dz^*} - \frac{\lambda L^2}{D}c^* + \frac{L^2 q}{Dc_\infty} = 0 \tag{5}$$

The three dimensionless parameters identified from Eq. (5) are

$$\pi_1(Pe) = \frac{uL}{D} \tag{6}$$

$$\pi_2 = \frac{\lambda L^2}{D} \tag{7}$$

$$\pi_3 = \frac{L^2 q}{Dc_\infty} \tag{8}$$

where π_1 is the Peclet number (Pe), a parameter that relates the effectiveness of mass transport by advection to dispersion or diffusion (Fetter, 1993). It is used for classifying transport regimes (Garges and Baehr, 1998; Huysmans and Dassargues, 2005; Haddad et al., 2012; Chattopadhyay and Pandit, 2015; Yadav et al., 2016), and also as a stability measure in numerical analysis (Ewing and Wang, 2001). For $\pi_1 < 1$, diffusion governs transport, and advection is negligible (Huysmans and Dassargues, 2005). For numerical or analytical studies, knowledge of the dominant transport mechanism helps to eliminate a hyperbolic term related to advection or parabolic terms related with diffusion.

Using boundary conditions

$$c(0) = c_o \tag{9}$$

$$c(L) = c_L \tag{10}$$

for a fracture with length of L, the solution to Eq. (4) is obtained as

$$c(z) = \frac{\left[c_L - \frac{q}{\lambda} - \left(c_o - \frac{q}{\lambda}\right)e^{\varsigma L}\right]e^{\Gamma z} - \left[c_L - \frac{q}{\lambda} - \left(c_o - \frac{q}{\lambda}\right)e^{\Gamma L}\right]e^{\varsigma z}}{e^{\Gamma L} - e^{\varsigma L}} + \frac{q}{\lambda} \tag{11}$$

where $\Gamma = \frac{u}{2D} + \sqrt{\frac{u^2}{4D^2} + \frac{\lambda}{D}}$ and $\varsigma = \frac{u}{2D} - \sqrt{\frac{u^2}{4D^2} + \frac{\lambda}{D}}$.

For clarity on the boundary conditions, Fig. 1 shows a schematic of a fractured rock with an arbitrarily located single fracture with the length of L, along the fracture axis (z). In this case, either end of the fracture can be c_o or c_L. If the flux is negative, then the transport direction is opposite to the assigned direction.

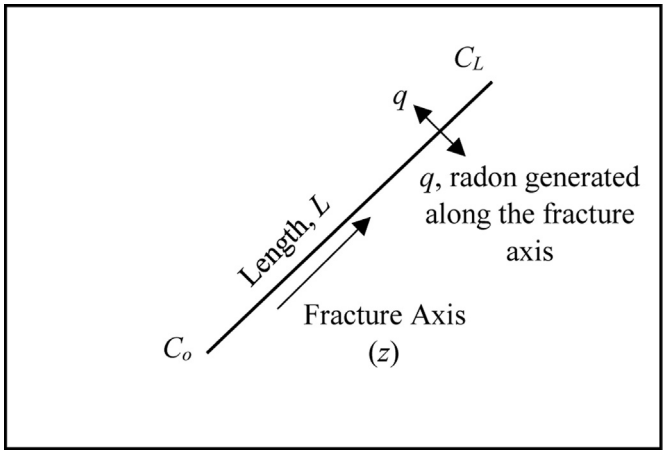

Fig. 1. Schematic of an arbitrarily located fracture within a rock domain.

2.1.3. Radon flux and dimensionless flux from a single fracture

Eq. (11) is included in Eqs. (1) and (2) to obtain the flux due to diffusion and advection at any point z as

$$J_{\text{diff}}(z) = -D\left\{\frac{\Gamma\left[c_L - \frac{q}{\lambda} - \left(c_o - \frac{q}{\lambda}\right)e^{\zeta L}\right]e^{\Gamma z} - \zeta\left[c_L - \frac{q}{\lambda} - \left(c_o - \frac{q}{\lambda}\right)e^{\Gamma L}\right]e^{\zeta z}}{e^{\Gamma L} - e^{\zeta L}}\right\} \tag{12}$$

$$J_{\text{adv}}(z) = u\left\{\frac{\left[c_L - \frac{q}{\lambda} - \left(c_o - \frac{q}{\lambda}\right)e^{\zeta L}\right]e^{\Gamma z} - \left[c_L - \frac{q}{\lambda} - \left(c_o - \frac{q}{\lambda}\right)e^{\Gamma L}\right]e^{\zeta z}}{e^{\Gamma L} - e^{\zeta L}} + \frac{q}{\lambda}\right\} \tag{13}$$

The total radon flux (J) at the end of a single fracture with length of L (Fig. 1) is obtained by summing (Andersen, 2001; Catalano et al., 2015) Eqs. (12) and (13) at $z = L$:

$$J(L) = c_L\delta + c_o\beta - q\varphi \tag{14}$$

where

$$\delta = \frac{1}{2}\left(u - \sqrt{u^2 + 4\lambda D}\coth\gamma\right) \tag{15}$$

$$\beta = \frac{e^{\frac{uL}{2D}}}{2}\left(\sqrt{u^2 + 4\lambda D}\ \operatorname{csch}\gamma\right) \tag{16}$$

$$\varphi = \frac{\delta + \beta - u}{\lambda} \tag{17}$$

where $\gamma = \sqrt{\left(\frac{uL}{2D}\right)^2 + \frac{\lambda L^2}{D}}$.

The dimensionless mass flux, J^*, is obtained by dividing Eq. (14) with the diffusion flux (Dc_∞/L):

$$J^* = \frac{c_L^*\pi_1(1 - \xi\coth\Psi)}{2} + \frac{c_o^*\pi_1 e^{0.5\pi_1}\,\xi\operatorname{csch}\Psi}{2} + \frac{\pi_3}{2\,\pi_2}\left(1 + \xi\coth\Psi - e^{0.5\pi_1}\,\xi\operatorname{csch}\Psi\right) \tag{18}$$

where $\xi = \sqrt{1 + 4\pi_2/(Pe)^2}$, $c_L^* = c_L/c_\infty$, $c_o^* = c_o/c_\infty$ and $\Psi = \sqrt{0.25(Pe)^2 + \pi_2}$.

2.1.4. Radon flux from a fracture network

Eq. (14) estimates radon flux from a single fracture; however, for a fracture network as shown in Fig. 2, the internal node concentrations are unknown (nodes 4 and 5), but specific values can be assigned to the boundary concentrations (nodes 1, 2 and 3).

Assuming that the boundary concentrations are known, the internal node concentration can be calculated using radon mass balance at each of the internal node:

$$\sum_{i=1}^{n} J_{i-j} = c_j\delta_{i-j} + c_i\beta_{i-j} - q\varphi_{i-j} = 0 \tag{19}$$

where n is the total number of nodes connected to a particular internal node, and j and i are the connecting nodes.

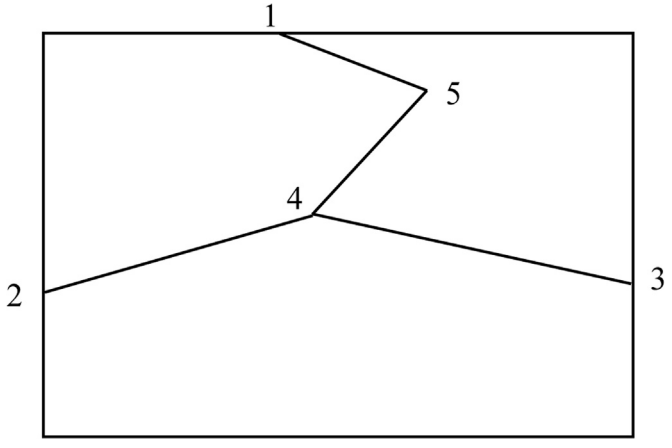

Fig. 2. Schematic of a typical fracture network.

For example, after applying Eq. (19) to nodes 4 and 5 in Fig. 2, we have

$$J_{2-4} + J_{5-4} + J_{3-4} = 0 \tag{20}$$

$$J_{4-5} + J_{1-5} = 0 \tag{21}$$

A linear set of equation is obtained as

$$\begin{bmatrix} \delta_{2-4} + \delta_{5-4} + \delta_{3-4} & \beta_{5-4} \\ \beta_{4-5} & \delta_{4-5} + \delta_{1-5} \end{bmatrix} \begin{bmatrix} C_4 \\ C_5 \end{bmatrix} = \begin{bmatrix} q(\varphi_{2-4} + \varphi_{5-4} + \varphi_{3-4}) - C_3\beta_{3-4} - C_2\beta_{2-4} \\ q(\varphi_{4-5} + \varphi_{1-5}) - C_1\beta_{1-5} \end{bmatrix} \tag{22}$$

Therefore, based on the number of internal nodes, say m, m number of equations that combines in the form of

$$\boldsymbol{AX} = \boldsymbol{B} \tag{23}$$

where $\boldsymbol{A}$ is the coefficient of the unknown internal node concentrations, $\boldsymbol{B}$ is the radon generation rate coefficient obtained mainly from the known boundary concentrations, and $\boldsymbol{X}$ is a matrix of the unknown internal node concentration. For a typical dense fracture network, a matrix system as large as 1200 × 1200 can be obtained, with each row of the matrix representing the application of Eq. (19) to the internal node. Due to the size of the system of equation, we solved for the internal node concentration in MATLAB using the 'mldivide' function.

2.1.5. Radon boundary flux

Fig. 3 shows the radon fluxes obtained based on the boundary gradients applied independently in two directions. J_{xx} and J_{yx} are the principal flux in the x direction and cross flux in the y direction, respectively; while J_{yy} and J_{xy} are the principal flux in the y direction and cross flux in the x direction, respectively. Unlike Fig. 2, in a typical fracture network, several fractures connect to the boundaries, and the total boundary flux is calculated as

$$J_{ij} = \sum_{i=1}^{N} (J_i A_i)/A_b \tag{24}$$

where N is the total number of fractures connecting to the particular boundary, A_i is the area of the specific fracture i (m^2), J_i is the corresponding flux (Bq/(m^2 s)), and A_b is the boundary area (m^2) (boundary length at a unit distance normal to the plane of flow (Priest, 2012a)). A_i depends on the aperture size, which affects flow and fluid transport (Nick et al., 2011). In a stochastic DFN model, the aperture sizes could be predicted by using the power-law distribution (De Dreuzy et al., 2001), assuming constant aperture (Min et al., 2004; Lei et al., 2014), and/or scaling the fracture aperture with length (Bonnet et al., 2001; Olson, 2003; Baghbanan and Jing, 2007; Klimczak et al., 2010; Bang et al., 2012). For most of the sections in this study, the aperture and length are correlated using (Klimczak et al., 2010):

$$\frac{4}{\pi} d_{avg} = \alpha_f L_t^{0.5} \tag{25}$$

$$\alpha_f = \frac{K_{IC}(1-\nu^2)}{E}\sqrt{\frac{8}{\pi}} \tag{26}$$

where d_{avg} is the hydraulic aperture (m), K_{IC} is the fracture toughness (MPa $m^{1/2}$), α_f is the proportionality coefficient considered as 0.0007 $m^{1/2}$ (Klimczak et al., 2010), ν is the Poisson's ratio, L_t is the length of the fractures (m), and E is the Young's modulus (MPa). This correlation is applicable to opening-mode fractures with constant fracture toughness (Klimczak et al., 2010).

It should be noted that α_f is a site-specific value and Eq. (25) is applicable when the rock is able to resist further fracturing. Therefore, in case of continuous fracturing, the driving stress is required to predict the fracture aperture. In this case, the hydraulic aperture can be predicted from (Pollard 1987; Olson, 2003):

$$\frac{4}{\pi} d_{avg} = \Delta\sigma_1 \frac{2(1-\nu^2)}{E} L_t \tag{27}$$

where $\Delta\sigma_1$ is the driving stress calculated from the normal stress and fluid pressure within the rock mass (MPa). Bisdom et al. (2016) calculated the driving stress based on the normal stress assuming constant fluid pressure as

$$\sigma_n = 0.5(\sigma_1 + \sigma_3) + 0.5(\sigma_1 + \sigma_3)\cos(2\beta) \tag{28}$$

where σ_1 is the maximum horizontal stress (assumed to be 30 MPa), σ_3 is the minimum horizontal stress (assumed to be 10 MPa), and β is the angle between fractures and direction of σ_1. This can increase the computational complexity; therefore, for most of this study, we used Eq. (25) to obtain the aperture sizes assuming constant fracture toughness. For clarity, it will be specified when the stress model is used to predict the aperture size.

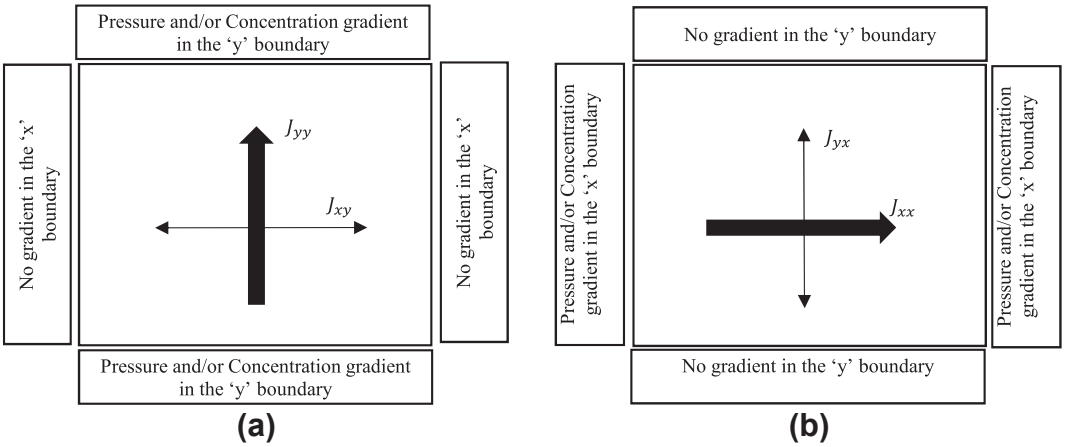

Fig. 3. (a) Applying concentration and/or pressure gradient in the y direction to obtain principal flux in the y direction (J_{yy}) and cross flux in the x direction (J_{xy}); and (b) Applying concentration and/or pressure gradient in the x direction to obtain principal flux in the x direction (J_{xx}) and cross flux in the y direction (J_{yx}).

2.2. Advection velocity

As observed in Section 2.1.3, advection velocity (u) is a required parameter for computing the radon flux (see Eq. (14)); three possible methods can be used to predict u. The first is by cubic law (Tsang, 1992; Xu and Dowd, 2010; Lee and Ni, 2015):

$$u = -\frac{\rho g}{\mu}\left(\frac{b^2}{12}\right)\frac{\Delta H}{L} \tag{29}$$

where ΔH is the pressure head difference (m), L is the length of the fractures (m), b is the fracture aperture (m), ρ is the density of air (kg/m^3), g is the acceleration due to gravity (m/s^2), and μ is the dynamic viscosity of air (N s/m^2). Since the internal pressure heads for the fractures are unknown, following cubic law is applied to estimate the pressure head at each of the internal nodes using the method suggested by Priest (Klimczak et al., 2010; Priest, 2012a):

$$Q = -\rho g b^3 (12\mu)^{-1}\,\nabla H \tag{30}$$

where Q is the volume flow rate (m^3/s). Although this approach is often used (Kohl et al., 1994; Mosley et al., 1996; van der Pal et al., 2001; Chauhan and Kumar, 2015; Datta, 2017), there are limited applications to contaminant transport through a DFN, and this is one of the contributions of this study (see Section 3.2.1). Fig. 4a shows a typical velocity distribution obtained from the cubic law model solving for airflow through a known DFN model (Priest, 2012a). The second approach calculates advection velocity from Eq. (6) for a specified Peclet number (Pe) and obtains a uniform velocity for each fracture. The third method assumes uniform advection velocity from previous studies such as the advection/diffusion model proposed by Benoit et al. (1991). Airflow study through a rock pile at Nordhalde (former uranium mining site of Ronneburg) obtained a velocity of 2.3148×10^{-6} m/s (Wels et al., 2003), while Nachshon et al. (2011) reported different advection velocities based on fracture aperture. Unlike the first approach, the second and third approaches assume uniform velocity distribution through the fracture network, as shown in Fig. 4b.

2.3. Discrete fracture network (DFN) model

Characterization of all fractures from a rock sample is impractical (Andersson and Dverstorp, 1987); therefore, a statistical approach is used. Previous studies considered stochastic DFN models in both two- and three-dimensional domains (Klimczak et al., 2010; Xu and Dowd, 2010; Jafari and Babadagli, 2012; Hyman et al., 2015; Liu et al., 2015; Ren et al., 2015), while some incorporated site data (Cacas et al., 1990; Min et al., 2004; Masihi et al., 2012; Dorn et al., 2013). In this study, a stochastic DFN model is developed for a two-dimensional (2D) domain. The parameters required for the model are locations of the fracture center, fracture orientation, fracture sets, fracture length, and fracture density. This section describes the approach used to develop the DFN in MATLAB.

The center of the fractures is modeled with uniform distribution (Parashar and Reeves, 2012; Priest, 2012b), and the orientation of the fractures is modeled with von Mises-Fisher distribution (Best and Fisher, 1979; Cacas et al., 1990; Parashar and Reeves, 2012; Reeves et al., 2012). Two fracture sets oriented at 0° and 90° are considered with a maximum trend variation of 30° (Klimczak et al., 2010). L_t is modeled using a power-law distribution:

$$L_t = L_{\min} U^{-1/a} \tag{31}$$

where $L_{\min}$ is the minimum length of fractures considered as 2 m (Klimczak et al., 2010), U is the uniform random variable that varies between 0 and 1, and a is the power law exponent assumed to be 2 with a corresponding fracture density (d_f) of 1.2 m/m^2 (Klimczak et al., 2010):

$$d_f = \sum_{i=1}^{N} L_{ti}/A_b \tag{32}$$

It is important to note that the model is very sensitive to the values of a. The length of the fractures generated decreases with increasing values of a. For example, $a = 1$ generates very long fractures; $a = 2$ generates a mix of short and long fractures; and $a = 3$ generates short fractures.

The fracture network is generated for a 2D domain until the fracture density in Eq. (32) is satisfied. After generating fractures in a DFN domain, we develop the DFN backbone by eliminating the dead ends. Fig. 5a shows a typical fracture network for a 40 m domain generated based on the method presented from MATLAB, and Fig. 5b shows the corresponding DFN backbone.

2.4. Numerical simulation

Fig. 5b is a typical example of the fracture network generated in this study. For a complex system like this, it is quite difficult to solve for the internal node concentration (Eq. (23)). Therefore, we developed a MATLAB function to

(1) Generate the stochastic DFN (Fig. 5a);
(2) Generate the DFN backbone (Fig. 5b);
(3) Classify the nodes as internal and external;

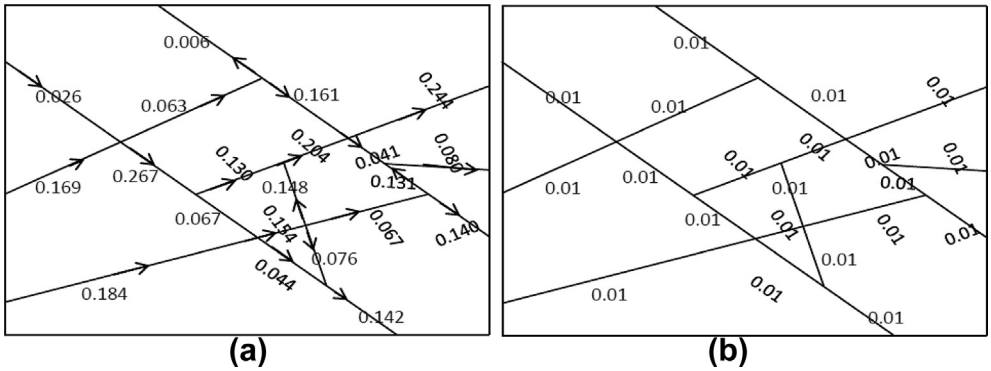

Fig. 4. DFN model presented by Priest et al. (2012a): (a) Example of airflow velocity (mm/s) for individual fractures obtained from cubic law; and (b) Constant values of advection velocity (mm/s) obtained from Eq. (6) or data from literature.

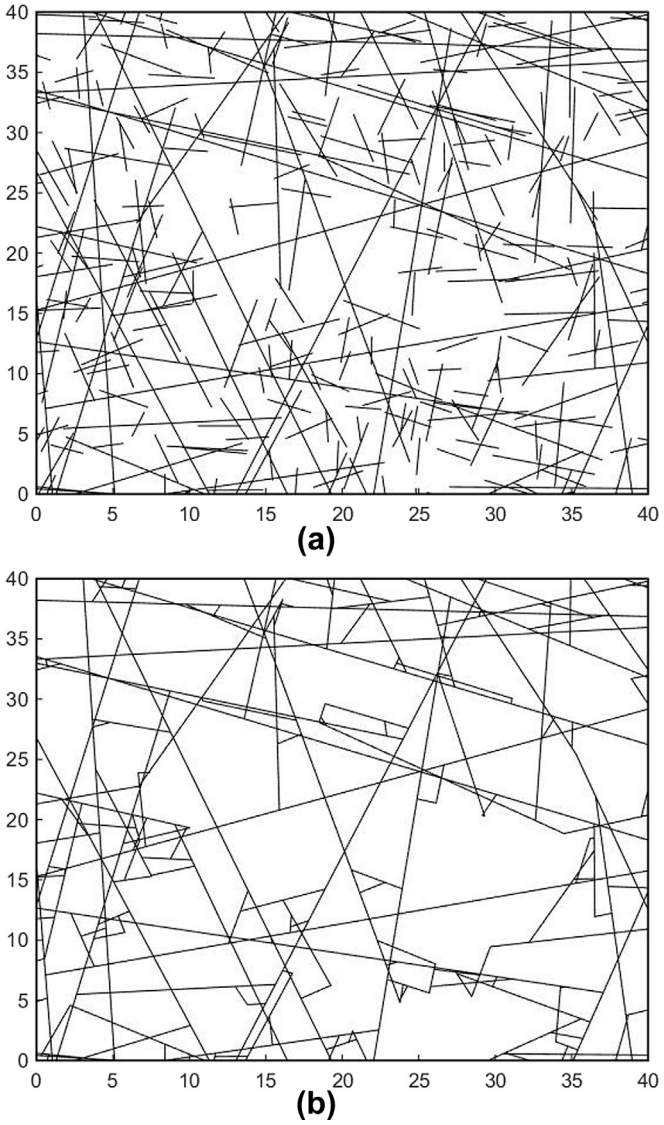

Fig. 5. (a) DFN generated for a 40 m domain; and (b) Corresponding DFN backbone (after eliminating the dead ends in Fig. 5a).

(4) Apply the boundary concentrations to the external nodes (Fig. 3);
(5) Calculate individual fracture advection velocity (Section 2.2);
(6) Apply mass balance to all internal nodes (Eq. (19));
(7) Form the matrix and solve the internal node concentration;
(8) Estimate boundary flux for a 2D domain.

Repeat steps (1)–(8) for Monte Carlo 100 simulations for any condition simulated, and an ensemble average of the 100 Monte Carlo simulations is presented for each of the results in Sections 3.1–3.3. A uniform radon generation rate (q) of 4.36 Bq/(m^3 s) is modeled using the fracture walls with a reference concentration c_∞ of 3,445,527 Bq/m^3 (Ye et al., 2014); radon diffusion coefficient (D) is modeled as 1.1×10^{-5} m^2/s (McPherson, 1993) through the fractures; and the decay coefficient is modeled as 2.1×10^{-6} s^{-1}.

2.5. Analytical model verification

A method for predicting the radon flux from fractured rocks using a DFN analysis is presented in this paper. However, due to the complexity of a typical DFN model (Fig. 5b), it is rather difficult to verify these results. As a result, we solved the transport equations analytically for a DFN configuration with a single fracture to determine a valid range of values used as a benchmark for the complex DFN model. The DFN model consists of a single horizontal fracture that runs through the width of the DFN domain (Fig. 6). Hence, the fracture length is equal to the domain length.

The minimum and maximum domain sizes considered are 2 m × 2 m and 150 m × 150 m, respectively. Using $\alpha_f = 0.0007$ m$^{1/2}$ in Eq. (25), the minimum and maximum hydraulic apertures are 7.78×10^{-4} m and 6.73×10^{-3} m, respectively. We used $q = 4.36$ Bq/(m^3 s) with a reference concentration of $c = 3,445,527$ Bq/m^3 and $c = 141,116$ Bq/m^3 (Ye et al., 2014). We analyzed the diffusion and advection models, independently. The diffusion flux is obtained by setting the velocity (u) to zero in Eq. (14) as

$$J_{\mathrm{dif}}(L) = -\sqrt{\lambda D}\left[c_L \coth\sqrt{\frac{\lambda}{D}}L - c_o \operatorname{csch}\sqrt{\frac{\lambda}{D}}L + \frac{q}{\lambda}\left(\operatorname{csch}\sqrt{\frac{\lambda}{D}}L - \coth\sqrt{\frac{\lambda}{D}}L\right)\right] \tag{33}$$

and the advection flux is obtained by the first eliminating diffusion in Eq. (3) as

$$u\frac{\partial c}{\partial z} + \lambda c - q = 0 \tag{34}$$

By applying the boundary condition, $c(0) = c_o$, the concentration is obtain as

$$c(z) = \left(c_o - \frac{q}{\lambda}\right)e^{-\frac{\lambda z}{u}} + \frac{q}{\lambda} \tag{35}$$

and the advection flux is obtained as

$$J_{\mathrm{adv}}(L) = u\left[c_o e^{-\frac{\lambda L}{u}} + \frac{q}{\lambda}\left(1 - e^{-\frac{\lambda L}{u}}\right)\right] \tag{36}$$

With the assumption of a constant radon generation rate, the only variable in the diffusion model (Eq. (33)) is the fracture length. Therefore, Eq. (33) is used to solve different fracture lengths (equal to the size of the DFN domain) as shown in Fig. 7a,b, using the minimum and maximum hydraulic apertures, respectively. The results show that diffusion flux decreases as the fracture length increases until about 40 m where the variation is minimized. This agrees with the previous knowledge of diffusion flux as we expect a decrease as the distance from the source increases (Eq. (1)). Based

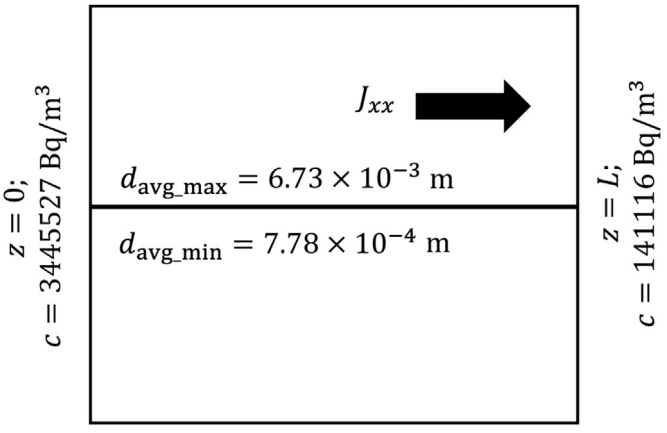

Fig. 6. Model used for verification of DFN model results from MATLAB.

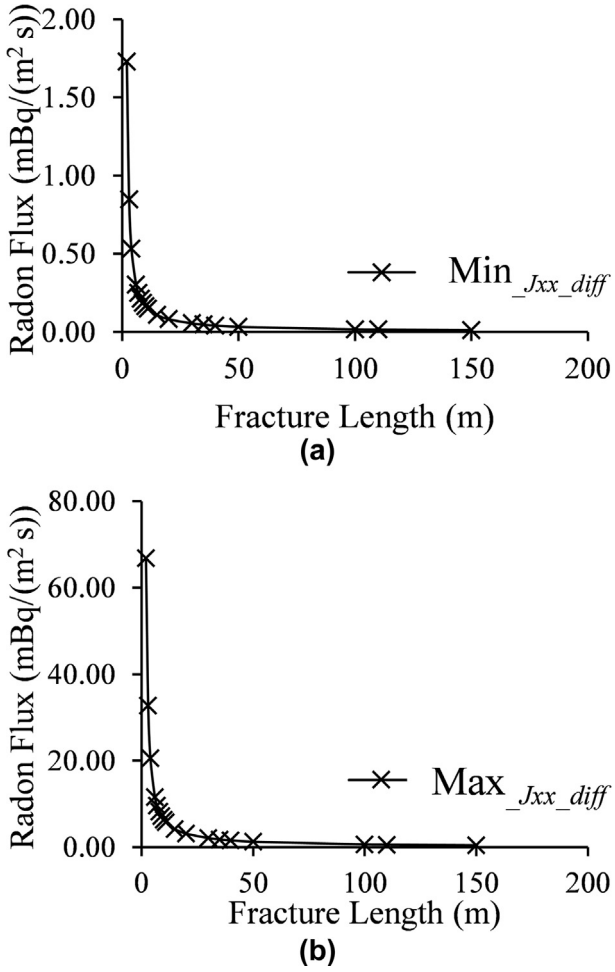

Fig. 7. (a) Plot of radon diffusion flux (calculated using minimum aperture) with the fracture length, Min_{Jxx_diff} represents the minimum principal diffusion flux; and (b) Plot of radon diffusion flux (calculated using maximum aperture) with the fracture length, Max_{Jxx_diff} represents the maximum principal diffusion flux.

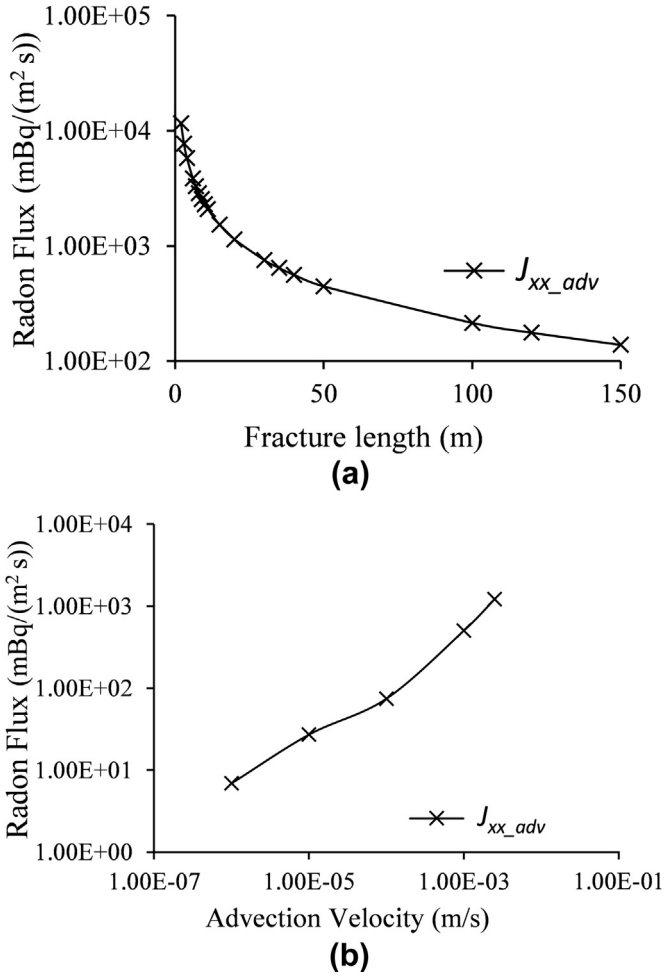

Fig. 8. J_{xx_adv} represents the principal advection flux in the x direction calculated with maximum aperture: (a) Effect of fracture length on radon advection flux; and (b) Radon advection flux (calculated using maximum aperture) with the advection velocity.

on Fig. 7a,b, we have a range that can be used to verify the results from the complex DFN model.

Eq. (36) predicts flux due to advection and has three variables as the fracture length, the advection velocity, and radon generation rate. Since a uniform radon generation rate is assumed, we studied the effects of advection velocity and fracture length on the advection flux using the maximum aperture size (6.73×10^{-3} m). Therefore, for a fixed advection velocity (1×10^{-3} m), the advection flux decreases with increase in fracture length to a minimum value (with slight variation beyond 40 m as shown in Fig. 8a). However, for a fixed fracture length (e.g. 2 m), Fig. 8b shows that the advection flux increases with an increase in advection velocity. These results agree with the existing knowledge on contaminant transport, and will be used to verify the results obtained from the DFN model.

3. Results and discussion

This section presents our findings based on the characteristics of the transport equation. Unless otherwise stated, the advection velocity is determined from Eq. (6) for a fixed Peclet number. Section 3.1 presents the radon mass flux for different DFN domains; Section 3.2 presents the sensitivity of the radon flux model to the DFN and transport parameters; and Section 3.3 presents radon dimensionless flux for a single fracture and a DFN.

3.1. Radon mass flux from DFN

As discussed in the Introduction, we highlighted some challenges associated with existing methods of predicting radon flux, a parameter that is required for effective mitigation. Here, we compare the effectiveness of our proposed method with previous work. Then, we also use our approach to determine the influence of domain sizes on radon flux measurements. The radon flux from the ADRE in Eq. (14) is solved for different DFN domain sizes (for example, the 40 m DFN domain in Fig. 5b) using zero advection velocity first (pure diffusion, $J_{yy\_no\_adv}$ in Fig. 9), and then with velocity computed from $\pi_1 = 1$ ($J_{yy\_diff\_adv}$ in Fig. 8a, equal effect of advection and diffusion).

Fig. 9 shows the results for both conditions using different DFN domains. We compared the results with the analytical model in Section 2.5, and observed that the range of values is similar to the analytical model, which is representative of values from previous studies (Singh et al., 1999; Sengupta et al., 2001; Mahur et al., 2008; Mudd, 2008). After verifying the range of values, we analyzed the trend of results based on the influences of advection, diffusion and

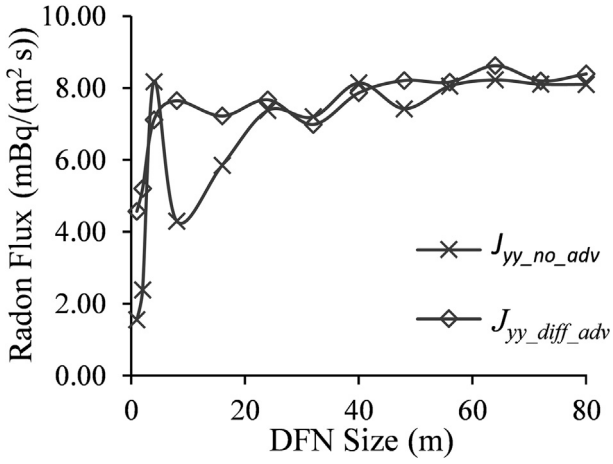

Fig. 9. Radon flux for different DFN sizes: comparison of radon fluxes for pure diffusion ($J_{yy\_no\_adv}$,$u = 0$ in Eq. (14)) with radon flux from both advection and diffusion (u is obtained from Eq. (6) with $\pi_1 = 1$, $J_{yy\_diff\_adv}$).

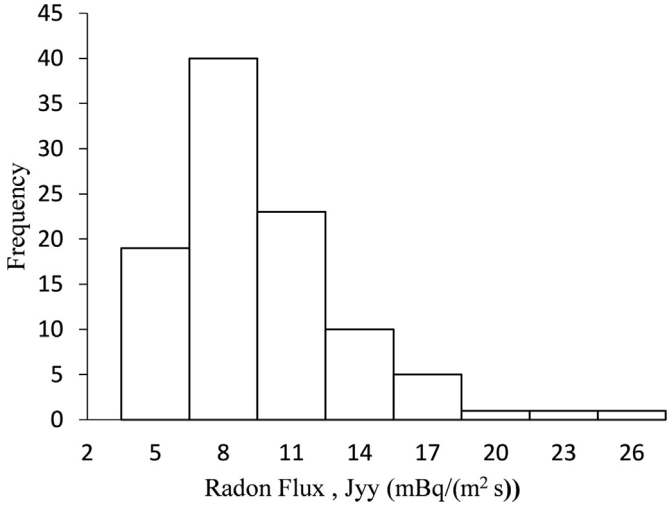

Fig. 10. Histogram of 100 Monte Carlo simulation results of radon flux for a 40 m DFN domain.

DFN size, which are some of the limitations in existing radon flux measurement approaches. For the diffusion model, radon flux increases as the size of the domain increases until about 8 m where it decreases. This can be attributed to the number of boundary fractures, and the diffusion length of radon. We understand that diffusion flux decreases with an increase in fracture length; however, as the DFN size increases, there is an increase in the number of boundary fractures (Fig. 5b). Therefore, based on Eq. (24), as N increases, the overall boundary diffusion flux increases. However, at a DFN size of about 8 m, we observe a decrease in flux as the effect of diffusion length outweighs the number of boundary fractures. Beyond the 8 m DFN domain, the radon flux increases slightly due to the increase in number of boundary fractures (Fig. 5b) until a 40 m DFN domain, where it is almost constant. At this point, even though the number of boundary fractures increases, the diffusion flux is significantly lower, and almost constant (Fig. 7a). Hence, at about 40 m, we establish a representative result for the DFN model.

Furthermore, in Fig. 9, the overall radon flux increases when both advection and diffusion are considered ($J_{yy\_diff\_adv}$), which is consistent with previous studies. Even though the effect of advection decreases with increasing fracture length, the increasing trend in the $J_{yy\_diff\_adv}$ plot is due to the increase in the number of boundary fractures, which increases with the DFN domain size. However, beyond 40 m, the flux remains almost constant, similar to the diffusion flux. In this sense, as the domain size increases, the average length of fractures in the domain increases, leading to a decrease in both diffusion and advection flux; however, the number of boundary fractures increases to maintain a constant flux. Recalling that the results presented in Fig. 9 are an average of 100 Monte Carlo simulations for each of the DFN domains, Fig. 10 shows the histogram of the range of radon flux magnitudes predicted for the 40 m DFN domain. We observe a few extreme values (more than double of the mean) as the model is right skewed. Since this model assumes a uniform advection velocity, the extreme values occur at very short fracture length around the DFN boundary due to the stochastic nature of a DFN. As presented in Figs. 7 and 8, radon fluxes are significantly higher with short fracture lengths. Therefore, further analysis is required for quantifying the uncertainty related to the stochastic model.

In reality, the advection velocity might vary significantly based on the pressure gradient across the domain. Therefore, we studied the effect of advection velocity on a 40 m DFN domain as shown in Fig. 11. The results show that an increase in the advection velocity increases radon flux through the DFN, which facilitates radon transport through fractured rock and shows that, in case of high advection velocity, the flux due to advection is significantly higher (Nilson et al., 1991; Rowberry et al., 2016). Therefore, a significant pressure gradient through the fractured rock boundaries can increase the radon flux into the environment. For this, pressure balancing through the fractured rock boundary is suggested as one of the proactive measures for radon mitigation in cave mines. These results provide conclusive evidence that our method agrees with existing studies, and beyond this, it is able to predict radon flux for large domain (which is a limitation for laboratory studies), and provide more insight into the contribution of fractures to radon flux.

3.2. Sensitivity of result to model parameters

After presenting the results in Section 3.1, it is necessary to study the sensitivity of the result to the parameters in the DFN and transport models. Some of these parameters are advection velocity model (u), aperture model (d_{avg}), fracture density (d_f), and radon generation rate (q).

3.2.1. Effect of advection velocity model on radon flux

Section 2.2 explains three different techniques for modeling advection velocity, but the results presented in Section 3.1 are based on uniform advection velocity calculated from Eq. (6).

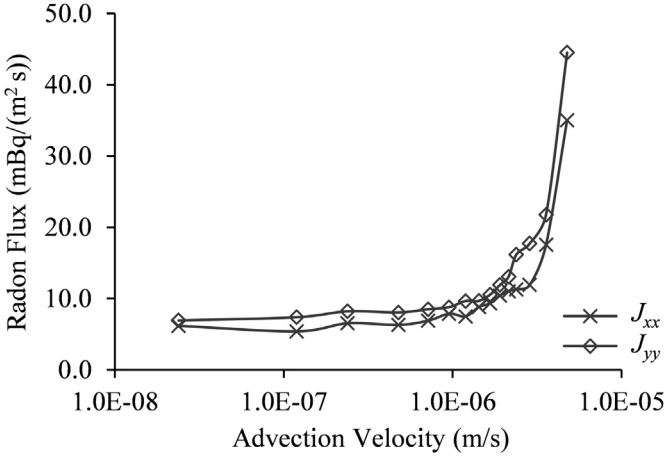

Fig. 11. Plot of radon flux with advection velocity for a 40 m DFN size.

Therefore, this section discusses the impact of different advection velocity models on the model results. First, we used the cubic law model from Eqs. (29) and (30) with a uniform aperture of 65 μm (Min et al., 2004) (different advection velocities generated for each fracture similar to Fig. 4a). Fig. 12a shows the radon flux for different DFN domain sizes. This figure shows that radon flux decreases until the DFN domain reaches about 40 m, with a small variation to assume a representative result. Though the trend to establish a representative result is different in Section 3.1 (Fig. 9), both methods show an insignificant change in radon flux in DFN models larger than 40 m in size. The difference in trend is due to the approach used to model the pressure head in Eq. (29). We maintained a constant pressure head difference (ΔH) for all the DFN sizes, and this decreases the advection velocity (Eq. (29)) as the domain size increases (which decreases the flux). Therefore, the model is sensitive to the advection velocity model implemented and the approach used. In addition, further investigation is needed to understand whether there might be differences in trend if the cubic law velocity model is implemented with a constant pressure head gradient ($\Delta H/L$) for each of the DFN domains.

For further analysis, we used a uniform velocity of 0.2 m/d (2.315×10^{-6} m/s) from the literature (Wels et al., 2003) as shown in Fig. 12b. The result shows a smooth trend towards the establishment of a representative result at a DFN domain of about 40 m similar to the result obtained previously. Since the effect of advection is assumed constant for each of the DFN sizes (uniform advection velocity), the slight increasing trend is due to the effect of diffusion as illustrated in Fig. 9.

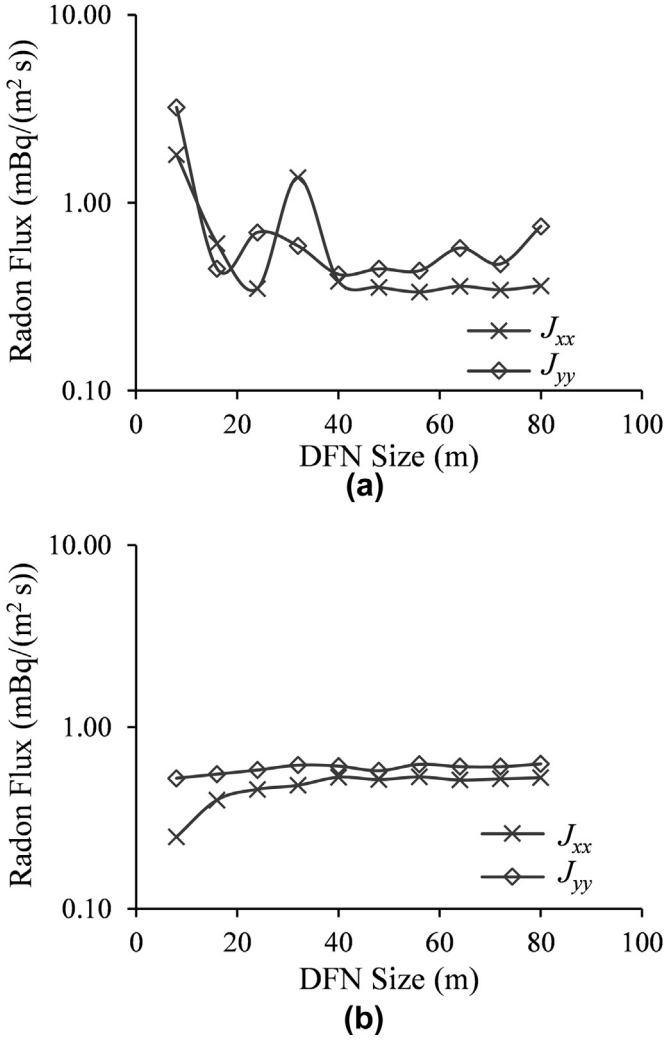

Fig. 12. Radon flux for ADRE solution with different advection velocity models: (a) Plot of radon flux for different DFN sizes with advection velocity obtained from cubic law; and (b) Plot of radon flux for different DFN sizes with advection velocity obtained from literature (uniform velocity).

3.2.2. *Effect of aperture model on radon flux*

Fracture aperture is a major source of uncertainty in fluid modeling (Bisdom et al., 2016) because small variation in the aperture has a significant effect on the flow modeling and contaminant transport properties (Nick et al., 2011). In the previous sections, we considered opening-mode fractures with a constant value of proportionality coefficient (α_f) used to correlate the fracture trace length with aperture (Eqs. (25) and (26)). However, from Eq. (26), α_f depends on the rock's properties such as Poison's ratio and Young's modulus, hence, it is site-specific. Klimczak et al. (2010) provided a summary of the proportionality coefficient for different sites, and three of these values are used to compare the variation in radon flux due to rock's mechanical properties. Fig. 13a compares the principal flux in the y direction, while Fig. 13b compare the cross flux in the x direction for 100 Monte Carlo simulations.

The results show that increase in values of α_f elevates the radon flux within several orders of magnitude. Therefore, rock properties such as fracture toughness, Poisson's ratio, and Young's modulus have significant effects on the size of the fracture opening (aperture), which affects the radon flux.

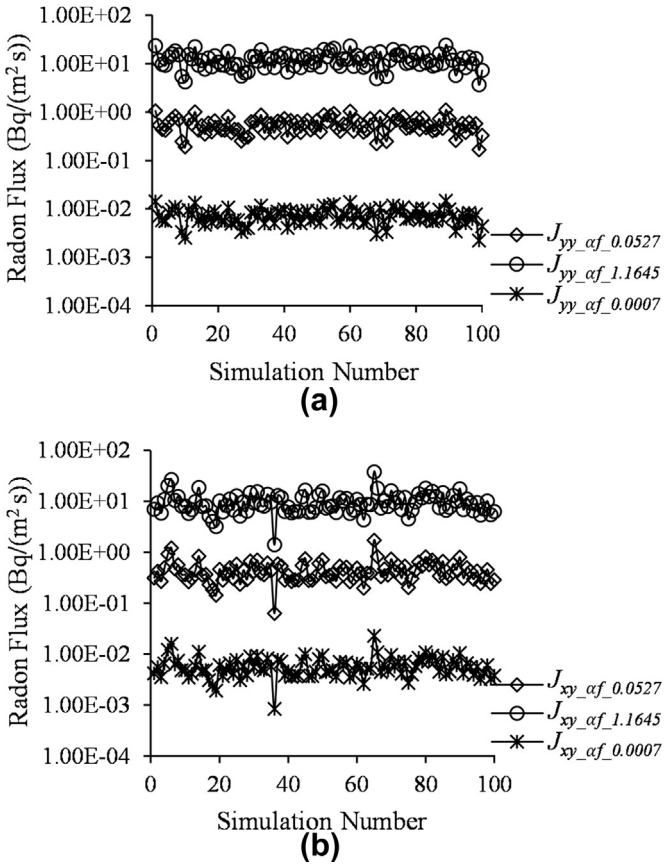

Fig. 13. (a) Comparison of radon principal flux in y direction for different values of α_f; and (b) Comparison of radon cross flux in x direction for different values of α_f. The legend displays radon flux along with the proportionality coefficient ($J_{yy\_\alpha f\_value}$); $J_{yy\_\alpha f\_0.0527}$ is the principal flux corresponding to $\alpha_f = 0.0527$ m$^{1/2}$ and $J_{xy\_\alpha f\_0.0527}$ is the cross flux corresponding to $\alpha_f = 0.0527$ m$^{1/2}$.

In most cases, considering the impact of stress on the aperture size is more realistic (as described in Section 2.1.5 with Eqs. (27) and (28)) than assuming a constant proportionality coefficient (α_f). Here, we compared the stress boundary conditions described in Eq. (28) with a constant value $\alpha_f = 0.0007\ m^{1/2}$ in Fig. 14. The result indicates that the stress aperture model (using Eq. (27)) shows more heterogeneity in the flux through the DFN compared to constant value of $\alpha_f = 0.0007\ m^{1/2}$ in Eq. (25) (the stress advection velocity model is able to replicate more realistic variation in the radon flux). Therefore, when rock properties such as α_f are not available, or the constant fracture toughness assumption is not valid, the stress boundary condition can be used in the model.

3.2.3. Effect of fracture density

One of the major parameters required for the DFN model is the fracture density (d_f) described in Eq. (32). In this study, we used $d_f = 1.2\ m/m^2$ for $a = 2$ (Klimczak et al., 2010); however, sometimes the rock might have a higher fracture density. Therefore, we analyzed the sensitivity of the model to the changes in fracture density for a DFN domain size of 40 m with uniformly distributed radon source. Fig. 15 shows the plot of radon flux with fracture density and an empirical relationship observed between both parameters. The model shows that about 10% increase in fracture density can increase the radon flux by about 15% due to the increase in porosity of the block, which creates more pathways for radon transport. Therefore, the model is very sensitive to the fracture density. In addition, a power relationship is observed between radon flux and fracture density. Although no unique fracture set is particularly related to a measured radon flux, the empirical relationship can be used with measured radon flux from field studies to predict an approximate fracture density for the rock.

3.2.4. Effect of radon generation rate

This model assumes a uniformly distributed radon source from the rock. However, different rocks have different average radon generation rates. Therefore, we studied the impact of changes in radon generation rate (q) between rock samples using a 40 m DFN domain. Fig. 16 shows that an increase in the generation rate increases radon flux, but not as significantly as changes in the fracture density as shown in Fig. 15. For example, there is a less than 10% increase in radon flux for the first 20% increase in q, which is unlike in Fig. 15. Therefore, for a rock sample with a uniformly distributed radon source, an increase in the fracture density has a more significant effect on radon flux compared to a rock with equivalent higher radon generation rate. Hence, a rock sample with a lower radon generation rate can be harmful if the fracture density is high.

3.3. Radon dimensionless flux

After presenting the results for radon flux, and discussing the model sensitivity to different parameters in Sections 3.1 and 3.2, this section focuses on radon dimensionless flux described in Eq. (18). Three dimensionless parameters are derived (i.e. Eqs. (6)–(8)) from Eq. (5). π_1 is a conventional dimensionless parameter (Peclet number), whereas π_2 and π_3 are dimensionless parameters derived from this study. For clarity, π_2 is named as dimensionless decay, and π_3, is named as dimensionless generation. Since both are dimensionless parameters presented in this study, it is important to study the range of values and their effects.

The dimensionless decay, π_2, is defined as the ratio of decay effect to diffusion effect:

$$\pi_2 = \frac{\text{Decay effect}}{\text{Diffusion effect}} \tag{37}$$

Since both λ and D are constants ($2.1 \times 10^{-6}\ s^{-1}$ and $1.1 \times 10^{-5}\ m^2/s$, respectively), the ratio of the decay constant to diffusion coefficient (λ/D) is 0.191. Therefore, the values depend significantly on the characteristic length, which could vary significantly depending

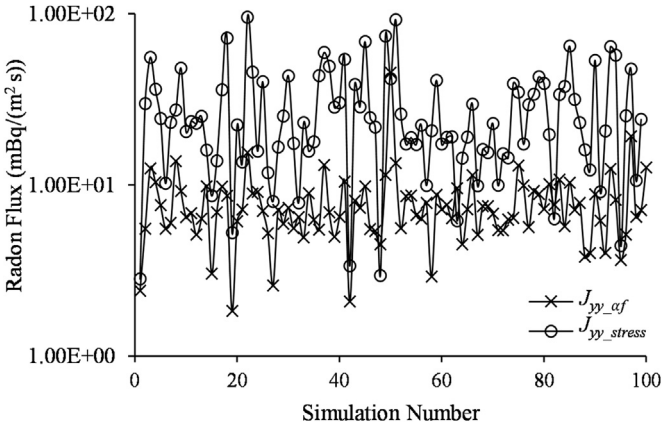

Fig. 14. Comparison of stress predicted from constant fracture toughness ($\alpha_f = 0.0007\ m^{1/2}$, J_{yy_af}) with variable stress condition (J_{yy_stress}).

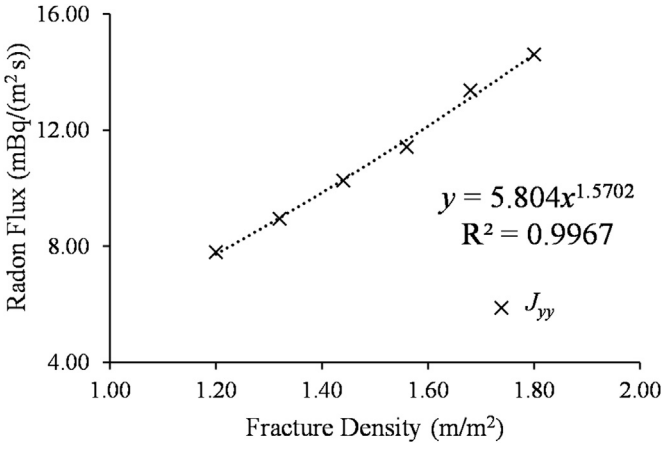

Fig. 15. Plot of radon flux with fracture density.

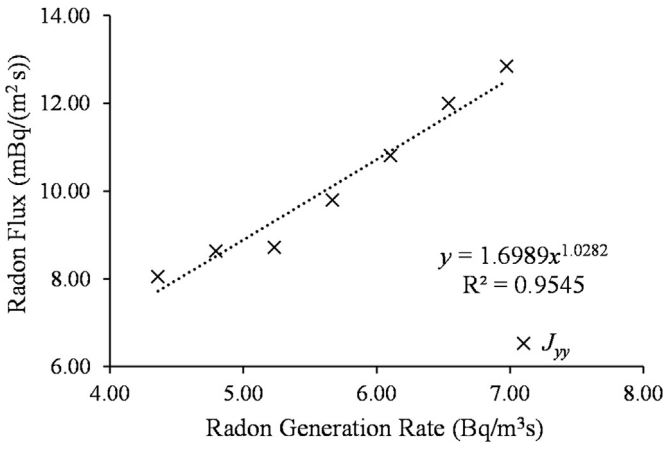

Fig. 16. Plot of radon flux with radon generation rate.

on the domain. For the characteristic length of 0.1 m, $\pi_2 \approx 0.00191$ and for 100 m, $\pi_2 \approx 1909$. However, using the diffusion length of radon (2.18 m), we have $\pi_2 \approx 0.91$. Hence, for $\pi_2 < 0.91$, diffusion transport is significant, and as π_2 increases significantly beyond 0.91, the effect of decay becomes more significant. Therefore, the radon flux decreases as π_2 increases.

The dimensionless generation π_3 is defined as the ratio of radon generation effect to the diffusion effect:

$$\pi_3 = \frac{\text{Generation effect}}{\text{Diffusion effect}} \tag{38}$$

Here, only the diffusion coefficient is a constant; hence, any of the other three values might vary to change π_3. For the values used in this study, we assumed $q/(Dc_\infty) \approx 0.12$. Using the diffusion length of radon as the characteristic length (2.18 m), it yields $\pi_3 \approx 0.55$. Therefore, $\pi_3 < 0.55$ implies that the concentration gradient is significant such that the mass flux due to the diffusion dominates the radon mass flux generated within the fracture walls. However, as π_3 increases, the radon generated within the fracture wall becomes very significant. Therefore, high values of π_3 imply high radon generation flux per unit distance, and vice versa.

3.3.1. Radon dimensionless flux for a single fracture

Here, we present the effect of the three dimensionless parameters on radon dimensionless flux for a single fracture. Fig. 17a shows the effect of π_1 on dimensionless flux for different values of π_2, and constant value of π_3 (=100). First, the result shows that an increase in π_1 significantly increases the dimensionless flux within 3–4 orders of magnitude for different values of π_2. Since the dimensionless flux is obtained by dividing the flux with the diffusion flux (Eq. (18)), as π_1 increases, the advection flux increases, and the dimensionless flux trends towards π_1. For a fixed value of π_1, radon dimensionless flux decreases with an increase in π_2. From Fig. 17a, we observed the minimum dimensionless flux for the highest value of π_2; hence, an increase in π_2 implies a significant effect of radon decay in the rock mass.

Similarly, we repeated the same study for different values of π_3 and π_2 (=1). This follows a similar trend as that in Fig. 17a, demonstrating that increase in π_1 increases radon dimensionless flux. However, in this case for a fixed π_1, an increase in π_3 elevates the radon dimensionless flux, and this implies an increase in the influence of radon generation rate within the rock mass. In addition, we observe that the range of variation increases for lower values of π_3, which indicates strong influence of diffusion.

3.3.2. Radon dimensionless flux for a DFN

Section 3.3.1 presents the effect of the dimensionless parameters on the dimensionless flux for a single fracture. However, in most cases, rocks consist of a network of fractures, hence, it is necessary to extend this to a fracture network. Therefore, this section focuses on the effects of dimensionless parameter on radon flux for a 40 m DFN domain. Fig. 18 shows the effect of π_1 on the dimensionless mass flux with constant values of $\pi_2 = 407$ and $\pi_3 = 245$ calculated using the maximum fracture length for the 40 m domain as $L = 46$ m. The result shows that radon dimensionless flux increases as the Peclet number increases similar to the single fracture study. The range of values varies within about 2 orders of magnitude unlike the single fracture effect in Fig. 17a due to the combined effects of the high value of π_2 in the fracture network. Therefore, increase in Peclet number increases radon dimensionless flux, but the range of influence depends on π_2.

Similarly, we studied the effect of π_2 on the dimensionless flux for a 40 m DFN domain as shown in Fig. 19. The result shows that increase in π_2 decreases radon dimensionless flux similar to the result obtained for a single fracture in Section 3.3.1. Furthermore, we studied the effect of π_3 on radon dimensionless flux for constant values of π_2 (= 407) (a DFN size of 40 m), and π_1 (= 1) as shown in Fig. 20. An increase in π_3 significantly increases the dimensionless flux (similar to results observed in Fig. 17b for a single fracture) due to the strong influnce of radon generation within the rock mass for high values of π_3. Therefore, for a DFN with constant π_1, the dimensionless flux decreases with an increase in π_2 for a fixed π_3, and the dimensionless flux increases with an increase in π_3 for a fixed π_2.

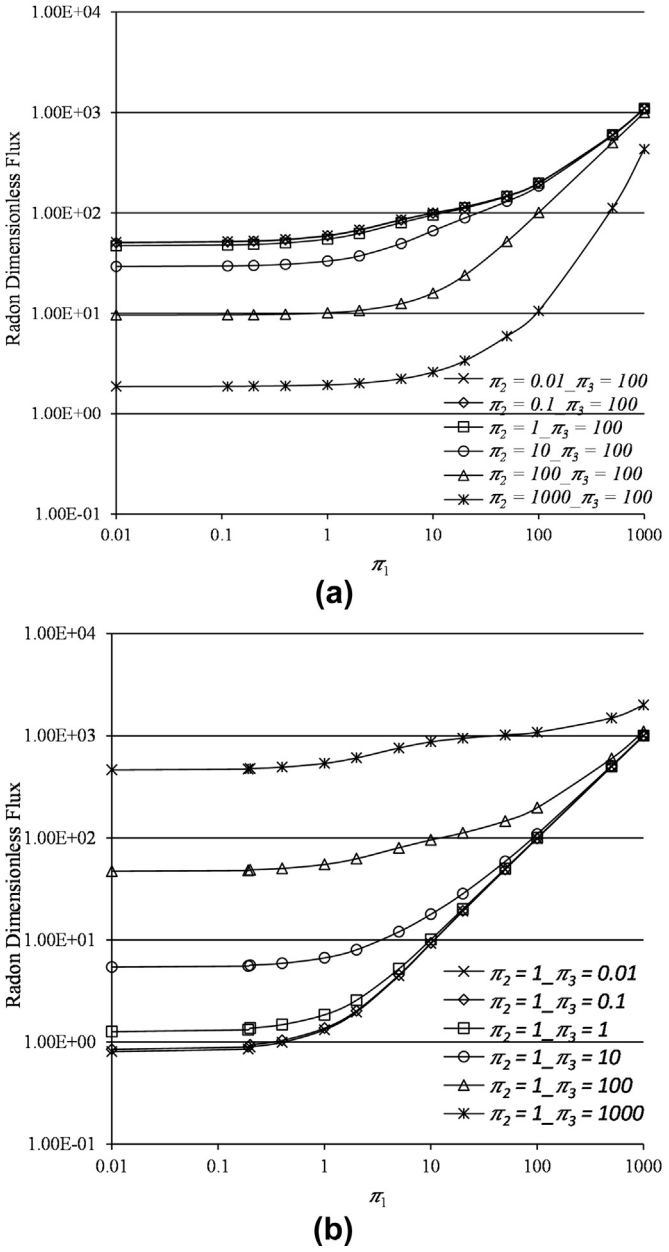

Fig. 17. Study of dimensionless flux for a single fracture. (a) Plot of dimensionless flux with Peclet number (π_1) for varying dimensionless decay (π_2) and constant dimensionless generation ($\pi_3 = 100$); and (b) Plot of dimensionless flux with Peclet number (π_1) for varying dimensionless generation (π_3) and constant dimensionless decay ($\pi_2 = 1$).

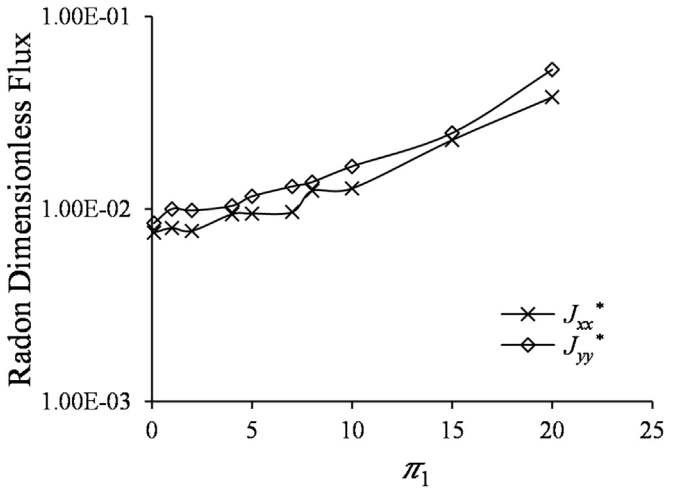

Fig. 18. Plot of dimensionless flux with Peclet number (π_1) with constant dimensionless decay ($\pi_2 = 407$) and dimensionless generation ($\pi_3 = 245$) for a DFN.

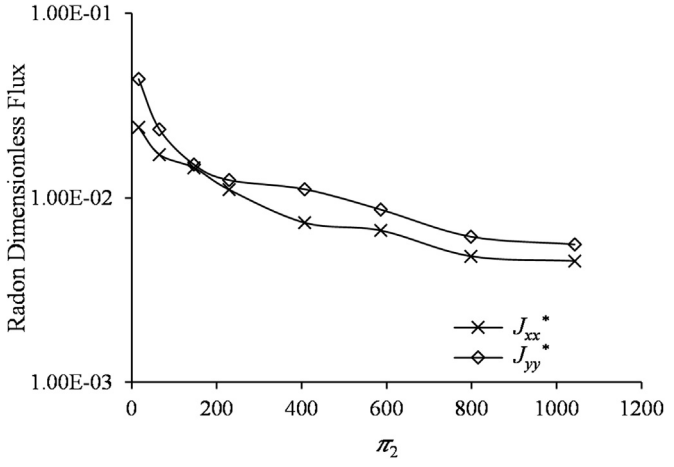

Fig. 19. Effect of dimensionless decay (π_2) on dimensionless flux with constant dimensionless Peclet number ($\pi_1 = 1$) and dimensionless generation ($\pi_3 = 245$) for a DFN.

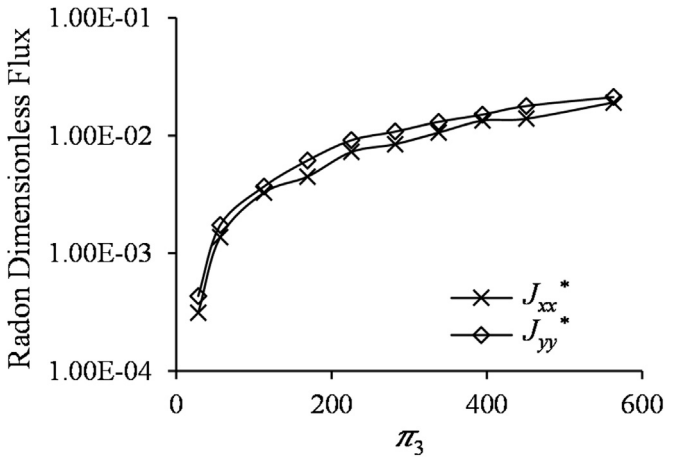

Fig. 20. Effect of dimensionless generation (π_3) on dimensionless flux with constant dimensionless Peclet number ($\pi_1 = 1$) and dimensionless decay ($\pi_2 = 407$) for a DFN.

4. Conclusions and future work

This paper presents an approach for determining radon flux from fractured rocks using a DFN model. This involves the derivation of radon flux equations related to transport due to advection and diffusion, application of radon mass balance, and generation of a stochastic DFN model. In cases of particular field study, discontinuity data from borehole, rock cores, and scanlines can be processed to identify fracture sets and their orientations to tune the stochastic model for better match of site-specific conditions. Therefore, this model predicts radon flux from fractured rocks, and it has specific application in rocks that are not easily accessible for field measurements.

In this study, we found that: (1) the proposed model predicts radon flux from fractured rock; (2) the model can be applied to specific locations if the site data such as fracture sets, fracture orientations, and rock's engineering properties are available; (3) the model is very sensitive to the advection velocity model and the aperture model implemented; (4) incorporating the effect of stress into the model shows more heterogeneity related to radon transport as observed from field studies; (5) an increase in fracture density increases radon flux, and an empirical power law relationship is found to relate both parameters; (6) the empirical relationship can be used with measured radon flux from field studies to predict the rock's fracture density; (7) radon flux increases with increase in radon generation rate, but not as sensitive as the fracture density, hence, increase in fracture density of a rock sample with uniformly distributed radon generation rate increases radon flux more than another rock sample with an equivalent increase in radon generation rate; (8) apart from Peclet number, a conventional dimensionless parameter and two other dimensionless parameters (π_2 and π_3) represent the effects of diffusion, radon generation and radon decay rate on radon dimensionless flux, respectively; (9) π_2 tagged dimensionless decay is defined as the ratio of decay effect to diffusion effect, and the increase in π_2 decreases radon dimensionless flux; and (10) π_3 tagged dimensionless generation is defined as the ratio of radon generation rate to diffusion rate, and increase in π_3 increases radon dimensionless flux.

Though we have developed a robust model to predict radon flux from fractured rocks, there are certain limitations to the model, which provides further opportunities for improvement. Some of these are: (1) implementing a distribution of radon generation rate within the rock mass since radon generation rate is not uniform in a real world scenario; (2) quantifying the uncertainty related to this model, since the results presented are averages of 100 Monte Carlo simulations, and there are uncertainties in the model due to the approach and input parameters used; (3) investigating the ratio of dimensionless generation to dimensionless decay within relevant transport regimes; (4) considering the interaction between the rock matrix and the DFN; and (5) implementing the model in three dimensions, and further investigation on the application of the identified dimensionless parameters. However, the numerical experience developed from this study shows that this model can predict radon flux from inaccessible zones, and also improve understanding of the radon transport mechanism through fractured rocks.

Conflicts of interest

The authors wish to confirm that there are no known conflicts of interest associated with this publication and there has been no significant financial support for this work that could have influenced its outcome.

Acknowledgements

The authors acknowledge the financial support from the National Institute for Occupational Safety and Health (NIOSH) (200-2014-59613) for conducting this research. The data for this paper are available at https://figshare.com/s/95560d8d59e72af7ef09.

Appendix A. Supplementary data

Supplementary data related to this article can be found at https://doi.org/10.1016/j.jrmge.2018.02.009.

References

Abumurad K, Al-Tamimi M. Emanation power of radon and its concentration in soil and rocks. Radiation Measurements 2001;34(1–6):423–6.
Andersen CE. Numerical modelling of radon-222 entry into houses: an outline of techniques and results. Science of the Total Environment 2001;272(1–3):33–42.
Andersson J, Dverstorp B. Conditional simulations of fluid flow in three-dimensional networks of discrete fractures. Water Resources Research 1987;23(10):1876–86.
Appleton JD. Radon in air and water. In: Essentials of medical geology. Springer; 2013. p. 239–77.
Baghbanan A, Jing L. Hydraulic properties of fractured rock masses with correlated fracture length and aperture. International Journal of Rock Mechanics and Mining Sciences 2007;44(5):704–19.
Bang SH, Jeon SW, Kwon SK. Modeling the hydraulic characteristics of a fractured rock mass with correlated fracture length and aperture: application in the underground research tunnel at Kaeri. Nuclear Engineering and Technology 2012;44(6):639–52.
Barakos G, Mischo H, Gutzmer J. Assessments of boundary conditions and requirements for rare earth underground mining due to presence of norms. In: Proceedings of the 1st European rare earth resources conference; 2014.
Bates R, Edwards J. Mathematical modeling of time dependent radon flux problems. In: Proceedings of the second international mine ventilation congress. New York: American Institute of Mining, Metallurgical, and Petroleum Engineers, Inc.; 1980.
Bear J, Tsang CF, Marsily GD. Flow and contaminant transport in fractured rocks. 1993.
Benoit JM, Torgersen T, O'Donnell J. An advection/diffusion model for ^{222}Rn transport in near-shore sediments inhabited by sedentary polychaetes. Earth and Planetary Science Letters 1991;105(4):463–73.
Best D, Fisher NI. Efficient simulation of the von Mises distribution. Journal of the Royal Statistical Society Series C (Applied Statistics) 1979;28(2):152–7.
Bisdom K, Bertotti G, Nick HM. The impact of different aperture distribution models and critical stress criteria on equivalent permeability in fractured rocks. Journal of Geophysical Research: Solid Earth 2016;121(5):4045–63.
Board M, Pierce M. A review of recent experience in modelling of caving. In: Proceedings of the international workshop on numerical modeling for underground mine excavation design; 2009.
Bochiolo M, Verdoya M, Chiozzi P, Pasquale V. Radiometric surveying for the assessment of radiation dose and radon specific exhalation in underground environment. Journal of Applied Geophysics 2012;83:100–6.
Bonnet E, Bour O, Odling NE, Davy P, Main I, Cowie P, Berkowitz B. Scaling of fracture systems in geological media. Reviews of Geophysics 2001;39(3):347–83.
Cacas M, Ledoux E, Marsily GD, Barbreau A, Calmels P, Gaillard B, Margritta R. Modeling fracture flow with a stochastic discrete fracture network: calibration and validation: 2. The transport model. Water Resources Research 1990a;26(3):491–500.
Cacas MC, Ledoux E, de Marsily G, Tillie B, Barbreau A, Durand E, Feuga B, Peaudecerf P. Modeling fracture flow with a stochastic discrete fracture network: calibration and validation: 1. The flow model. Water Resources Research 1990b;26(3):479–89.
Catalano R, Immé G, Mangano G, Morelli D, Aranzulla M. Radon transport: laboratory and model study. Radiation Protection Dosimetry 2015;164(4):575–81.
Chattopadhyay A, Pandit SK. A peclet number based analysis of mixed convection for lid-driven porous trapezoidal enclosure. Procedia Engineering 2015;127:628–35.
Chauhan RP, Kumar A. A comparative study of indoor radon contributed by diffusive and advective transport through intact concrete. Physics Procedia 2015;80:109–12.
Cigna AA. Radon in caves. International Journal of Speleology 2005;34(1):1–18.
Datta D. An algorithm for solving fuzzy advection diffusion equation and its application to transport of radon from soil into buildings. International Journal of System Assurance Engineering and Management 2017;8(S4):2129–36.
De Dreuzy JR, Davy P, Bour O. Hydraulic properties of two-dimensional random fracture networks following a power law length distribution: 1. Effective connectivity. Water Resources Research 2001;37(8):2065–78.
Dorn C, Linde N, Le Borgne T, Bour O, de Dreuzy JR. Conditioning of stochastic 3-D fracture networks to hydrological and geophysical data. Advances in Water Resources 2013;62:79–89.
El-Fawal M. Mathematical modelling for radon prediction and ventilation air cleaning system requirements in underground mines. Journal of American Science 2011;7(2):389–402.
Ewing RE, Wang H. A summary of numerical methods for time-dependent advection-dominated partial differential equations. Journal of Computational and Applied Mathematics 2001;128(1):423–45.
Ferry C, Richon P, Beneito A, Cabrera J, Sabroux JC. An experimental method for measuring the radon-222 emanation factor in rocks. Radiation Measurements 2002;35(6):579–83.
Fetter CW. Mass transport in saturated media contaminant hydrogeology, vol. 500. Macmillan publishing company; 1993.
Garges JA, Baehr AL. Type curves to determine the relative importance of advection and dispersion for solute and vapor transport. Ground Water 1998;36(6):959–65.
Haddad AS, Hassanzadeh H, Abedi J. Advective-diffusive mass transfer in fractured porous media with variable rock matrix block size. Journal of Contaminant Hydrology 2012;133:94–107.
Holford DJ, Schery SD, Wilson JL, Phillips FM. Modeling radon transport in dry, cracked soil. Journal of Geophysical Research: Solid Earth 1993;98(B1):567–80.
HPA. Radon and public health: report prepared by the subgroup on radon epidemiology of the independent advisory group on ionising radiation, documents of the health protection agency. UK: Health Protection Agency; 2009.
Huysmans M, Dassargues A. Review of the use of Péclet numbers to determine the relative importance of advection and diffusion in low permeability environments. Hydrogeology Journal 2005;13(5–6):895–904.
Hyman JD, Karra S, Makedonska N, Gable CW, Painter SL, Viswanathan HS. dfnWorks: a discrete fracture network framework for modeling subsurface flow and transport. Computers & Geosciences 2015;84:10–9.
Iakovleva VS, Ryzhakova NK. A method for estimating the convective radon transport velocity in soils. Radiation Measurements 2003;36(1–6):389–91.
Jafari A, Babadagli T. Estimation of equivalent fracture network permeability using fractal and statistical network properties. Journal of Petroleum Science and Engineering 2012;92–93:110–23.
Kitto M. Radon testing in schools in New York State: a 20-year summary. Journal of Environmental Radioactivity 2014;137:213–6.
Klimczak C, Schultz RA, Parashar R, Reeves DM. Cubic law with aperture-length correlation: implications for network scale fluid flow. Hydrogeology Journal 2010;18(4):851–62.
Kohl T, Medici F, Rybach L. Numerical simulation of radon transport from subsurface to buildings. Journal of Applied Geophysics 1994;31(1–4):145–52.
Lario J, Sánchez-Moral S, Canaveras J, Cuezva S, Soler V. Radon continuous monitoring in Altamira Cave (northern Spain) to assess user's annual effective dose. Journal of Environmental Radioactivity 2005;80(2):161–74.
Lee IH, Ni CF. Fracture-based modeling of complex flow and CO_2 migration in three-dimensional fractured rocks. Computers & Geosciences 2015;81:64–77.
Lei Q, Latham JP, Xiang J, Tsang CF, Lang P, Guo L. Effects of geomechanical changes on the validity of a discrete fracture network representation of a realistic two-dimensional fractured rock. International Journal of Rock Mechanics and Mining Sciences 2014;70:507–23.
Li L, Tang C, Zhao X, Cai M. Block caving-induced strata movement and associated surface subsidence: a numerical study based on a demonstration model. Bulletin of Engineering Geology and the Environment 2014;73(4):1165–82.
Liu R, Jiang Y, Li B, Wang X. A fractal model for characterizing fluid flow in fractured rock masses based on randomly distributed rock fracture networks. Computers and Geotechnics 2015;65:45–55.
Mahur A, Kumar R, Sonkawade R, Sengupta D, Prasad R. Measurement of natural radioactivity and radon exhalation rate from rock samples of Jaduguda uranium mines and its radiological implications. Nuclear Instruments and Methods in Physics Research Section B: Beam Interactions with Materials and Atoms 2008;266(8):1591–7.
Masihi M, Sobhani M, Al-Ajmi AM, Al-Wahaibi YM, Al-Wahaibi TK. A physically-based three dimensional fracture network modeling technique. Scientia Iranica 2012;19(3):594–604.
McNearny R, Abel J. Large-scale two-dimensional block caving model tests. International Journal of Rock Mechanics and Mining Sciences & Geomechanics Abstracts 1993;30(2):93–109.
McPherson MJ. Radiation and radon gas. In: Subsurface ventilation and environmental engineering. Springer; 1993. p. 457–87.
Min KB, Jing L, Stephansson O. Determining the equivalent permeability tensor for fractured rock masses using a stochastic REV approach: method and application to the field data from Sellafield, UK. Hydrogeology Journal 2004;12(5):497–510.
Mosley R, Menetrez M, Snoddy R, Brubaker S. The influences of diffusion and advective flow on the distribution of radon activity within USEPA's soil chamber. Environment International 1996;22(1S):521–33.
Mudd GM. Radon releases from Australian uranium mining and milling projects: assessing the UNSCEAR approach. Journal of Environmental Radioactivity 2008;99(2):288–315.
Nachshon U, Weisbrod N, Dragila MI, Ganot Y. The importance of advective fluxes to gas transport across the earth-atmosphere interface: the role of thermal convection. INTECH Open Access Publisher; 2011.

Nadakavukaren A. Our global environment: a health perspective. Waveland Press; 2011.
Nazaroff WW, Nero AV. Radon and its decay products in indoor air. 1988.
Nick H, Paluszny A, Blunt M, Matthai S. Role of geomechanically grown fractures on dispersive transport in heterogeneous geological formations. Physical Review E 2011;84:056301.
Nilson R, Peterson E, Lie K, Burkhard N, Hearst J. Atmospheric pumping: a mechanism causing vertical transport of contaminated gases through fractured permeable media. Journal of Geophysical Research: Solid Earth 1991;96(B13):21933–48.
Olson JE. Sublinear scaling of fracture aperture versus length: an exception or the rule? Journal of Geophysical Research: Solid Earth 2003;108(B9).
Ongori JN, Lindsay R, Newman RT, Maleka PP. Determining the radon exhalation rate from a gold mine tailings dump by measuring the gamma radiation. Journal of Environmental Radioactivity 2015;140:16–24.
Parashar R, Reeves DM. On iterative techniques for computing flow in large two-dimensional discrete fracture networks. Journal of Computational and Applied Mathematics 2012;236(18):4712–24.
Pollard D. Theoretical displacements and stresses near fractures in rock: with applications to faults, joints, veins, dikes, and solution surfaces. Fracture Mechanics of Rock 1987:277–349.
Prasad G, Ishikawa T, Hosoda M, Sorimachi A, Janik M, Sahoo SK, Tokonami S, Uchida S. Estimation of radon diffusion coefficients in soil using an updated experimental system. Review of Scientific Instruments 2012;83(9):093503.
Priest SD. Fluid flow in discontinuities. In: Discontinuity analysis for rock engineering. Springer Science & Business Media; 2012a. p. 340–81.
Priest SD. Discontinuity size. In: Discontinuity analysis for rock engineering. Springer Science & Business Media; 2012b. p. 150–96.
Reeves DM, Parashar R, Zhang Y. Hydrogeologic characterization of fractured rock masses intended for disposal of radioactive waste. INTECH Open Access Publisher; 2012. p. 351–72.
Ren F, Ma G, Fu G, Zhang K. Investigation of the permeability anisotropy of 2D fractured rock masses. Engineering Geology 2015;196:171–82.
Rowberry MD, Martí X, Frontera C, Van De Wiel MJ, Briestenský M. Calculating flux to predict future cave radon concentrations. Journal of Environmental Radioactivity 2016;157:16–26.
Sahu P, Mishra DP, Panigrahi DC, Jha V, Patnaik RL. Radon emanation from low-grade uranium ore. Journal of Environmental Radioactivity 2013;126:104–14.
Sainsbury B. Sensitivities in the numerical assessment of cave propagation. In: Potvin Y, editor. Proceedings of the 2nd international symposium on block and sublevel caving; 2010.
Schery S, Gaeddert D, Wilkening M. Transport of radon from fractured rock. Journal of Geophysical Research: Solid Earth 1982;87(B4):2969–76.
Sengupta D, Kumar R, Singh A, Prasad R. Radon exhalation and radiometric prospecting on rocks associated with Cu–U mineralizations in the Singhbhum shear zone, Bihar. Applied Radiation and Isotopes 2001;55(6):889–94.
Singh A, Sengupta D, Prasad R. Radon exhalation rate and uranium estimation in rock samples from Bihar uranium and copper mines using the SSNTD technique. Applied Radiation and Isotopes 1999;51(1):107–13.
Thompkins R. Radiation in uranium mines. Part 1. Bulletin of the Canadian Institute of Mining and Metallurgy 1982;75(845):149–56.
Tsang Y. Usage of "equivalent apertures" for rock fractures as derived from hydraulic and tracer tests. Water Resources Research 1992;28(5):1451–5.
US EPA. Health risk of radon. Retrieved August 2nd, 2017, from: https://www.epa.gov/radon/health-risk-radon.
van der Pal M, van der Graaf E, de Meijer R, de Wit M, Hendriks N. Experimental set-up for measuring diffusive and advective transport of radon through building materials. Science of the Total Environment 2001;272(1–3):315–21.
Wels C, Lefebvre R, Robertson AM. An overview of prediction and control of air flow in acid-generating waste rock dumps. In: Proceedings of the 6th international conference on acid rock drainage; 2003.
Xie D, Wang H, Kearfott KJ. Modeling and experimental validation of the dispersion of ^{222}Rn released from a uranium mine ventilation shaft. Atmospheric Environment 2012;60:453–9.
Xu C, Dowd P. A new computer code for discrete fracture network modelling. Computers & Geosciences 2010;36(3):292–301.
Yadav N, Yadav A, Kim JH. Numerical solution of unsteady advection dispersion equation arising in contaminant transport through porous media using neural networks. Computers & Mathematics with Applications 2016;72(4):1021–30.
Ye YJ, Wang LH, Ding DX, Zhao YL, Fan NB. Inverse method for determining radon diffusion coefficient and free radon production rate of fragmented uranium ore. Radiation Measurements 2014;68:1–6.
Zhang W, Zhang D, Wang X, Xu M, Wang H. Analysis of mathematical model for migration law of radon in underground multilayer strata. Mathematical Problems in Engineering 2014.

Dr. Kayode Ajayi obtained his BS degree from Obafemi Awolowo University, and MS degree from South Dakota School of Mines and Technology (SDSM&T). He graduated in May 2018 with a doctorate degree from the Department of Mechanical Engineering, SDSM&T. During his studies at SDSM&T, he worked as graduate research assistant in the Department of Mining Engineering and Management. Dr. Ajayi's expertise is in numerical analysis of radon transport through fractured rocks and cave mines. He has presented his findings in several international conferences with peer-reviewed proceedings.